This is an open access article published under an ACS AuthorChoice License, which permits copying and redistribution of the article or any adaptations for non-commercial purposes.

JACS
JOURNAL OF THE AMERICAN CHEMICAL SOCIETY

Article

pubs.acs.org/JACS

An Endoperoxide Reactivity-Based FRET Probe for Ratiometric Fluorescence Imaging of Labile Iron Pools in Living Cells

Allegra T. Aron,[†] Morten O. Loehr,[†] Jana Bogena,[†] and Christopher J. Chang*[,†,‡,§]

[†]Department of Chemistry, [‡]Department of Molecular and Cell Biology, and [§]Howard Hughes Medical Institute, University of California, Berkeley, Berkeley, California 94720, United States

Supporting Information

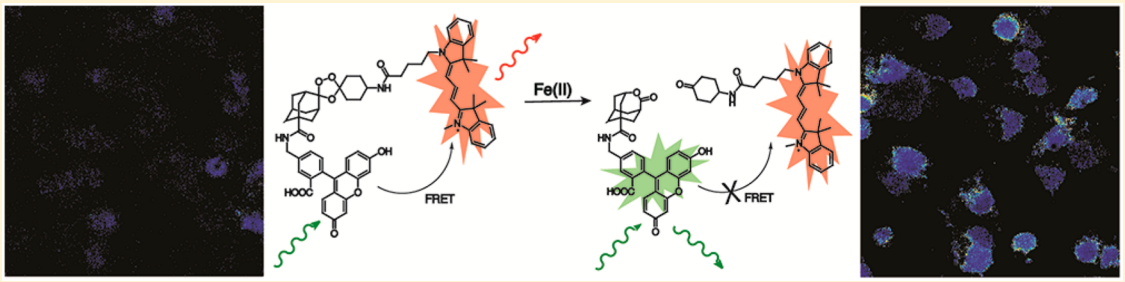

ABSTRACT: Iron is essential for sustaining life, as its ability to cycle between multiple oxidation states is critical for catalyzing chemical transformations in biological systems. However, without proper regulation, this same redox capacity can trigger oxidative stress events that contribute to aging along with diseases ranging from cancer to cardiovascular and neurodegenerative disorders. Despite its importance, methods for monitoring biological iron bound weakly to cellular ligands—the labile iron pool—to generate a response that preserves spatial and temporal information remain limited, owing to the potent fluorescence quenching ability of iron. We report the design, synthesis, and biological evaluation of FRET Iron Probe 1 (FIP-1), a reactivity-based probe that enables ratiometric fluorescence imaging of labile iron pools in living systems. Inspired by antimalarial natural products and related therapeutics, FIP-1 links two fluorophores (fluorescein and Cy3) through an Fe(II)-cleavable endoperoxide bridge, where Fe(II)-triggered peroxide cleavage leads to a decrease in fluorescence resonance energy transfer (FRET) from the fluorescein donor to Cy3 acceptor by splitting these two dyes into separate fragments. FIP-1 responds to Fe(II) in aqueous buffer with selectivity over competing metal ions and is capable of detecting changes in labile iron pools within living cells with iron supplementation and/or depletion. Moreover, application of FIP-1 to a model of ferroptosis reveals a change in labile iron pools during this form of cell death, providing a starting point to study iron signaling in living systems.

INTRODUCTION

Iron is a required element for all living organisms and is the most abundant transition metal in the human body.[1−4] Its ability to cycle between multiple oxidation states is essential for carrying out a diverse array of unique functions in biological systems, spanning nucleotide synthesis to oxygen transport to electron transfer.[5,6] However, this same potent redox activity makes iron in unregulated forms potentially toxic to the cell, owing to its ability to promote oxidative stress by participating in processes like the Fenton reaction where iron-catalyzed disproportionation of hydrogen peroxide can generate hydroxyl radical and other harmful reactive oxygen species.[7] Indeed, misregulation of iron levels has been linked to diseases associated with aging,[8] including cardiovascular[9] and neurodegenerative disorders,[10,11] and a variety of cancers.[12−15] As such, the cell employs intricate systems for maintaining iron homeostasis, and a ferrous iron pool that is bound weakly to cellular ligands—defined as the labile iron pool—exists at the center of this dynamic network.

Despite its central importance, methods for noninvasive detection of labile Fe(II) within living cells and other intact biological specimens remain limited,[16,17] owing to intrinsic properties of Fe(II) as a weak binder on the Irving−Williams series[18] and as a potent fluorescence quencher by electron and/or energy transfer.[19,20] Indeed, the majority of sensors and probes for Fe(II) either lack selectivity for Fe(II) over other biologically relevant metal ions as well as oxidation state specificity over Fe(III), and/or lose spatial resolution due to their "turn-off" fluorescence readout.[21,22] To address the dual issues of selectivity and Fe(II)-dependent quenching, we[23] and others[24,25] have pursued reactivity-based approaches[26−30] to labile iron detection by a "turn-on" response, where an Fe(II)-selective reaction with a caged dye leads to release of the parent fluorophore without permanent iron binding. Inspired by bioinorganic oxidations mediated by heme and nonheme iron enzymes, our laboratory reported Iron Probe 1 (IP1), a reactivity-based probe for Fe(II) that makes use of an iron-mediated, oxygen-dependent dealkylation to trigger a turn-on response.[23] While this probe was highly specific for Fe(II) and

Received: August 2, 2016
Published: October 21, 2016

© 2016 American Chemical Society

DOI: 10.1021/jacs.6b08016
J. Am. Chem. Soc. 2016, 138, 14338−14346

Scheme 1. Design of FRET Iron Probe (FIP-1)

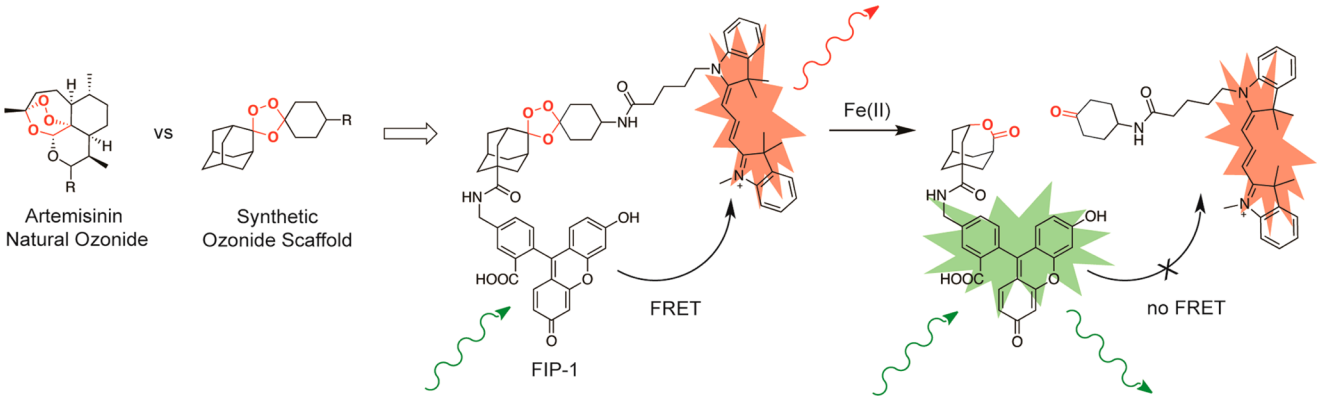

Scheme 2. Synthesis of FRET Iron Probe FIP-1[a]

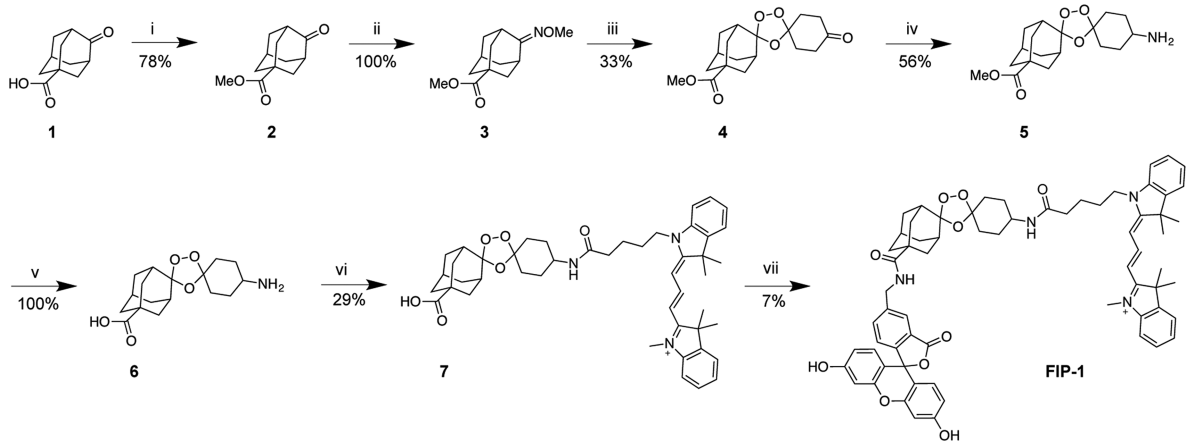

[a]Reagents and conditions: (i) $SOCl_2$, MeOH, 0 °C to r.t., 12 h; (ii) H_2NOMe-HCl, pyridine, r.t., 3 h; (iii) 1,4-cyclohexanedione, O_3, CH_2Cl_2, CCl_4, 0 °C, 2.5 h; (iv) NH_4OAc, $NaBH_3CN$, MeOH r.t., 12 h; (v) LiOH, THF, H_2O, r.t., 12 h; (vi) Cy3-NHS ester, NEt_3, DMF, 30 °C, 12 h; (vii) 5-aminomethyl fluorescein, HBTU, DIPEA, DMF, r.t., 12 h.

was capable of monitoring changes in endogenous labile iron pools, it required three components (probe, Fe(II), and O_2) to produce a change in signal. We envisioned an improved detection platform that could exhibit oxygen-independent reactivity and give a fluorescence response that directly reports on reaction with Fe(II). In addition, we sought to introduce a ratiometric readout,[31−34] which enables internal self-calibration through multiple excitation/emission profiles to minimize interferences arising from analyte-independent phenomena such as sample thickness, heterogeneity and/or variations in light intensity.

We now report the design, synthesis, and biological application of a first-generation ratiometric fluorescent probe for Fe(II) by modulating fluorescence resonance energy transfer (FRET) between two dyes linked by an Fe(II)-responsive trigger. Specifically, FRET Iron Probe 1 (FIP-1) exploits an Fe(II)-cleavable endoperoxide linker inspired by antimalarial and anticancer drug scaffolds, which achieve specificity for parasites and tumors via elevations in local iron concentrations,[35−43] to control FRET between donor and acceptor dyes. This chemical design strategy is generally applicable to a broad range of ratiometric or turn-on probes for selective detection of iron or other chemical analytes that are potent fluorescent quenchers. FIP-1 features high selectivity and sensitivity to Fe(II) over competing biologically relevant metals and is capable of monitoring changes in labile iron pools in living cells in situations of iron excess and/or deficiency. The ratiometric readout of this probe also facilitates comparative screening of labile iron levels across a variety of cell types, identifying cancer cell types that possess higher basal levels of labile iron. Finally, the application of FIP-1 to a model of ferroptosis enables, to the best of our knowledge, the first direct imaging evidence of changes in labile iron stores upon induction of this form of cell death. This result provides a starting point for further studies of iron as a transition metal signal in biology.[44]

RESULTS AND DISCUSSION

Design and Synthesis of FIP-1. Our design of FIP-1 makes use of an endoperoxide moiety prominent in natural antimalarial agents such as artemisinin[35] and synthetic endoperoxide variants.[45−47] We envisioned creating an Fe(II)-responsive FRET platform with two fluorophores linked through an endoperoxide core. In the absence of iron, FRET would proceed efficiently through the intramolecular donor and acceptor pair. Fe(II)-mediated cleavage of the endoperoxide bridge would then result in dissociation of the two fluorophores from each other and concomitant loss of FRET signal (Scheme 1). We chose a 5-aminomethyl fluorescein (5-AMF) donor and a cyanine 3 (Cy3) acceptor as a FRET pair owing to their spectral overlap and broad utility as dyes in biological

DOI: 10.1021/jacs.6b08016
J. Am. Chem. Soc. 2016, 138, 14338−14346

imaging.[48,49] We note that this basic chemical strategy can be generalized to other fluorophore/fluorophore and fluorophore/quencher pairs, in addition to other modalities including photoacoustic, chemiluminescent, bioluminescent, MRI, and PET, for selective detection of iron and other analytes where quenching by a permanent binding event might present a challenge for generating a signal that preserves spatial resolution. When FIP-1 is intact, FRET occurs between 5-AMF and Cy3 when the probe is excited at the fluorescein excitation maximum. Upon Fe(II)-mediated cleavage of the endoperoxide linker, FRET no longer occurs between the dissociated 5-AMF and Cy3 moieties, resulting in an increase in 5-AMF emission at 515 nm. Increases in labile Fe(II) can then be monitored using the ratio of emission profiles for 5-AMF and Cy3, which we designate hereafter as Green/FRET ratio.

The synthesis of FIP-1 is described briefly as follows. The dual-functionalized adamantyl-endoperoxide linker was synthesized in five steps from a commercially available starting material (Scheme 2). 2-Adamantanone-5-carboxylic acid **1** was converted to the methyl ester **2** through a Fischer esterification and this mixture was subsequently treated with hydroxylamine-hydrochloride to afford oxime ether **3**. Oxime **3** was then treated with 1,4-cyclohexanedione and ozone in a Griesbaum co-ozonolysis reaction to afford endoperoxide **4**. Reductive amination was carried out on endoperoxide **4** followed by subsequent saponification to afford the endoperoxide-carboxylic acid linker **6**. Cy3-NHS-ester and 5-AMF were synthesized using published procedures.[50,51] With these key pieces in hand, Cy3-NHS-ester and 5-AMF were coupled sequentially onto the dual-functionalized linker to yield FIP-1 (Scheme 2).

Reactivity and Fe(II) Selectivity of FIP-1 in Aqueous Buffer. With FIP-1 in hand, its fluorescence response to Fe(II) was evaluated in aqueous buffer (50 mM HEPES, pH 7.4). As expected, FIP-1 shows absorption maxima at 495 and 545 nm, corresponding to 5-AMF and Cy3, respectively, (Figure S1, dashed line) with molar attenuation coefficients of ε_{495} = 24 800 M^{-1} cm^{-1} and ε_{543} = 27 800 M^{-1} cm^{-1} (Figure S2), emission maxima at 515 and 556 nm (Figure 1a, dashed line), and a FRET efficiency of ca. 85% based on analysis of the separate donor and acceptor fragments compared to the full intact probe (Figure S3). When exposed to Fe(II), FIP-1 exhibits an increase in 5-AMF-derived emission at 515 nm (Figure 1a, solid line and S1, solid line). Notably, the increase in 5-AMF emission partially obscures the anticipated decrease in Cy3 acceptor emission centered at 556 nm resulting from the loss in intramolecular FRET owing to spectral overlap.

The observed increase in Green/FRET ratio is consistent with loss of FRET by endoperoxide cleavage with Fe(II), as supported by both UV−vis signatures (Figure S1), and mass spectrometry data that confirm the presence of an intact endoperoxide before Fe(II) reaction and 5-AMF and Cy3 derived fluorophore components after Fe(II) reaction. This FRET change reaches saturation within ca. 90 min when 1 μM FIP-1 is treated with 10 μM Fe(II) in aqueous buffer (Figure S4a) and exhibits fast reaction kinetics with a pseudo-first order rate constant of 0.0016 s^{-1} (Figure S4b). At a concentration of 1 μM FIP-1, FIP-1 is also capable of sensing low levels of Fe(II) in aqueous buffer in a dose-dependent manner (Figure S5).

We next evaluated the selectivity of FIP-1 for Fe(II) compared to a panel of biologically relevant transition, alkali, and alkaline earth metals (Figure 1b). The data show that FIP-1 exhibits a highly metal- and oxidation state-specific response to Fe(II) and gives negligible FRET change in the presence of

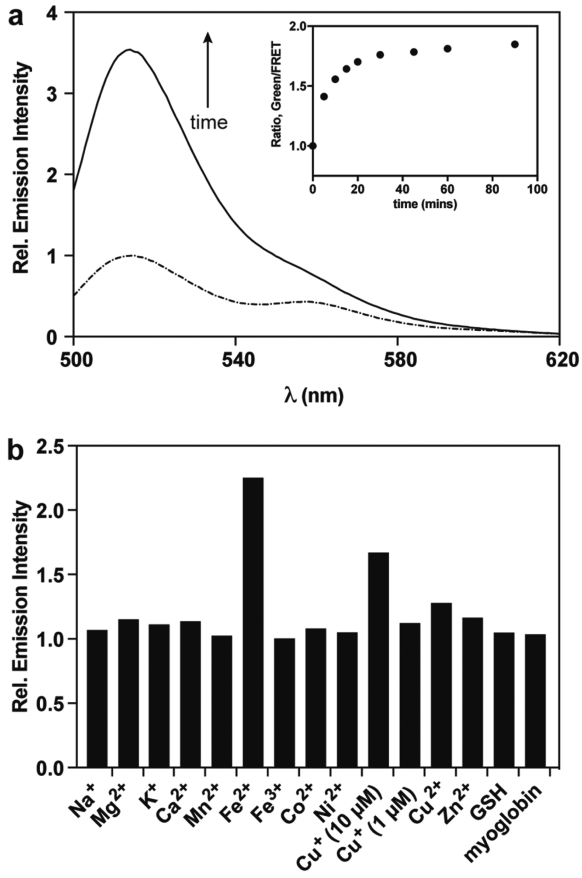

Figure 1. (a) Fluorescence intensity of 1 μM FIP-1 before (dashed line) and after (solid line) reaction with 10 μM Fe(II) at time = 90 min. Ratio change over time is shown as an inset. (b) Fluorescence response of 1 μM FIP-1 to biologically relevant d-block (10 μM) and s-block (1 mM) metals as well as to glutathione (GSH) (5 mM) and myoglobin (10 μM). Manipulations were performed anaerobically and spectra were acquired at 37 °C in 50 mM HEPES (pH 7.4) when monitoring intensity of the 5-AMF donor, with λ_{ex} = 488 nm, collecting emission between 500−620 nm.

glutathione, the major intracellular reductant (Figure 1b). Only Cu(I) at 10 μM levels gives a modest response, but FIP-1 is not responsive to lower concentrations of Cu(I) (1 μM). These data, combined with the ca. 10-fold higher abundance of iron over copper in the typical eukaryotic cell,[1,52,53] coupled with the relatively high buffering capacity of the cell for copper in the form of glutathione and metallochaperones (pM-fM K_d values),[54−58] suggest FIP-1 has a sufficient *in vitro* selectivity profile for application to labile iron detection in biological systems. Indeed, while FIP-1 responds to addition of 10 μM Fe(II) in HEK 293T cells (Figure S6), FIP-1 shows no response to addition of 10 μM Cu(I) in HEK 293T, indicating that FIP-1 is selective for labile iron over Cu(I) *in cellulo* (Figure S7).

Application of FIP-1 to Imaging Labile Iron Pools in Living Cells. Having established the ability of FIP-1 to respond selectively to physiological Fe(II) levels in aqueous buffer,[22,53] we next explored its ability to respond to changes in Fe(II) levels in living cells through ratiometric fluorescence imaging. The data establish that FIP-1 is indeed able to visualize both increases and decreases in intracellular Fe(II) levels. HEK 293T cells exposed to 100 μM Fe(II) for 90 min, treated with FIP-1 for 90 min, and then imaged showed a patent increase in

DOI: 10.1021/jacs.6b08016
J. Am. Chem. Soc. 2016, 138, 14338−14346

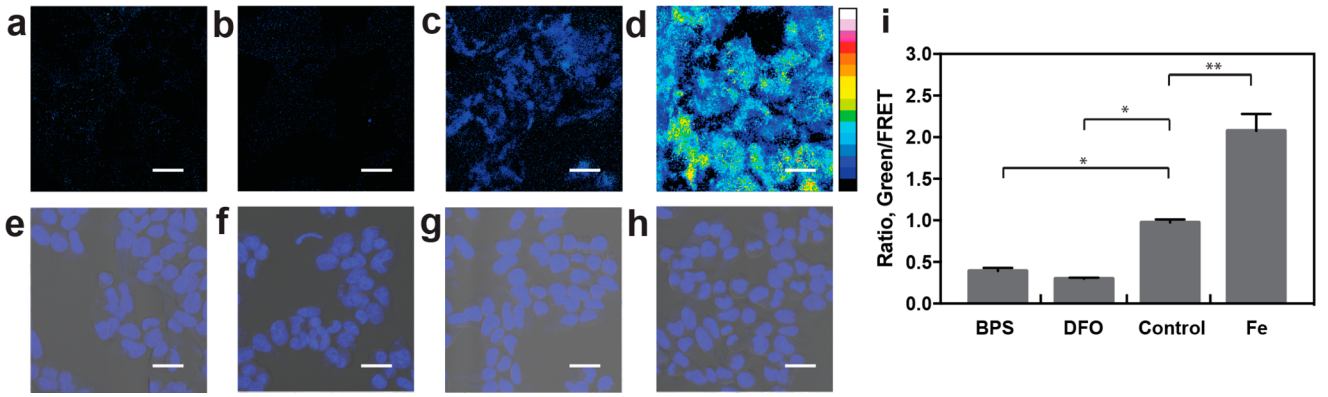

Figure 2. Representative ratiometric confocal microscopy images of live HEK 293T cells loaded with FIP-1. Cells were treated with (a) 1 mM bathophenanthroline disulfonate (BPS) for 9.5 h, (b) 250 μM deferoxamine (DFO) for 9.5 h, (c) vehicle, or (d) 100 μM ferrous ammonium sulfate (FAS) for 90 min. Cells were washed and treated with 10 μM FIP-1 in HBSS for 90 min then washed 2× with HBSS before acquiring images. (e–h) Brightfield images of (a–d) overlaid with Hoechst stain. (i) Mean Green/FRET ratios of HEK 293T cells treated with Fe(II) and chelators; error bars denote SEM, $n = 3$. Statistical significance was assessed by calculating p-values using one-way ANOVA with the Bonferroni correction in R, $^{*}p < 0.05$, $^{**}p < 0.01$. Scale bar = 25 μm.

Green/FRET ratio over control cells. In contrast, HEK 293T cells pretreated either with 1 mM bathophenanthroline disulfonate (BPS)—a ferrous iron chelator—or with 250 μM deferoxamine (DFO)—a ferric iron chelator—for 9.5 h then stained with FIP-1 for 90 min exhibited a decrease in Green/FRET ratio when compared to control cells (Figure 2). Chelator concentrations and incubation times were chosen based on pilot ICP-MS data that suggested decreased cellular iron levels under these conditions. However, we note that FIP-1 is also able to visualize changes in labile Fe(II) levels in cells that have been treated with lower chelator dosages (Figure S8). Indeed, as a control, the iron addition treatments used in the above imaging experiments were independently shown to alter total levels of intracellular iron by inductively coupled plasma mass spectrometry (ICP-MS) (Figure S9), consistent with the interpretation that FIP-1 is responding to the altered iron levels in these treatments. Furthermore, FIP-1 showed a dose-dependent response with varying levels of Fe(II) (Figure S6), but not a concentration dependence for FIP-1 itself (Figure S10). Finally, cell viability during these treatments in both the absence and the presence of FIP-1 was verified by propidium iodide staining, which confirmed that the cell viability was not significantly affected under these conditions compared to the vehicle control (Figure S11 and S12). Although offering an advantage over turn-off probes that give a loss of signal upon Fe(II) detection, we note a potential limitation in the first-generation FIP-1 FRET cleavage design where over longer time periods the fragments resulting from the Fe(II)-mediated endoperoxide cleavage can diffuse away from the site of reaction with Fe(II).

After verifying that FIP-1 was able to detect both increases and decreases in labile Fe(II) pools in a dose-dependent manner in HEK 293T cells, we sought to generalize its applicability to assay labile Fe(II) levels in other cell types. Owing to emerging interest in the connections between iron homeostasis and cancer,[12,59−61] we chose to compare the normal human mammary epithelial MCF10A cell line and two cancer lines, the metastatic human breast adenocarcinoma MDA-MB-231 cell line and the human osteocarcinoma U2OS cell line (Figure 3). Interestingly, we observe that the FIP-1 Green/FRET ratio is significantly higher in MDA-MB-231 and U2OS cells under basal states compared to the normal breast

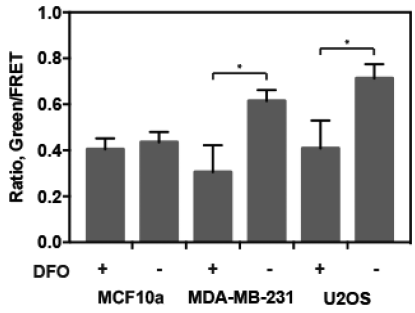

Figure 3. Application of FIP-1 to assay labile iron content across a variety of cell lines. Data shown for MCF10A normal breast cells compared to MDA-MB-231 and U2OS cancer cells under basal conditions and after treated with 250 μM DFO for 8 h. Cells were washed, stained with 10 μM FIP-1 in HBSS for 90 min, then washed 2× with HBSS before acquiring images. Mean Green/FRET ratio was obtained for each cell line; error bars denote SEM, $n = 3$. Statistical significance was assessed by calculating p-values using one-way ANOVA with the Bonferroni correction in R, $^{*}p < 0.05$.

cell line MCF10A, consistent with reports that suggest expansion of iron pools in tumor cells[12,47,62,63] over normal healthy ones. Moreover, treatment of the two cancer cell lines with 250 μM DFO for 8 h attenuates the FRET responses to levels comparable of the MCF10A cells with or without DFO treatment, presaging that this expanded labile iron pool can be specifically targeted in cancer cells while leaving normal cells relatively unaltered in terms of iron status. Taken together, the data establish that FIP-1 is responsive to changes in endogenous levels of labile Fe(II) across multiple cell types and can be potentially used to screen across a variety of cell types.

FIP-1 Enables Identification of Changes in Labile Iron Status in a Model of Ferroptosis. With results showing that FIP-1 is capable of assaying relative levels of labile iron pools within a given cell type under basal conditions and situations of iron overload or iron deficiency, as well as compare cell types, we sought to explore the application of FIP-1 to directly observe potential changes in labile Fe(II) levels in cells undergoing ferroptosis. Ferroptosis refers to a novel and biochemically, genetically, and morphologically distinct form of cell death that can be triggered in cancer cells with a structurally

DOI: 10.1021/jacs.6b08016
J. Am. Chem. Soc. 2016, 138, 14338−14346

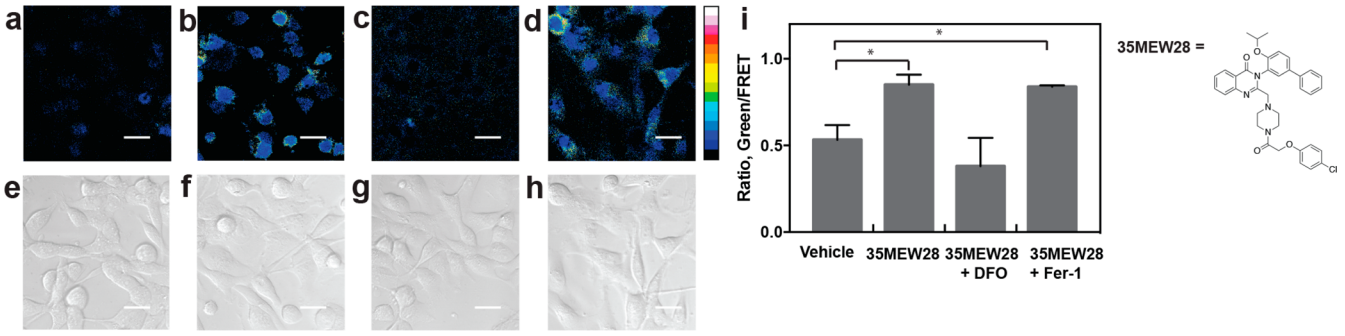

Figure 4. FIP-1 enables direct detection of changes in labile iron pools upon induction of ferroptosis. Confocal microscopy of 10 μM FIP-1 in MDA-MB-231 cells treated with (a) vehicle, (b) 1.25 μM 35MEW28 (see structure above) for 8 hours, (c) 1.25 μM 35MEW28 + 100 μM DFO for 8 hours, and (d) 1.25 μM 35MEW28 + 1 uM Fer-1 for 8 hours. (e-h) Brightfield images of (a-d). (i) Mean Green/FRET ratios of MDA-MB-231 cells treated with ferroptosis-inducing compounds and inhibitors; error bars denote SEM, $n = 3$. Statistical significance was assessed by calculating p-values using one-way ANOVA with the Bonferroni correction in R, $^*p < 0.05$. Scale bar = 25 μm.

diverse class of small molecules.[64] Cell death is suggested to be iron-dependent, as treatment with iron chelators reverses the death phenotype. Death was shown to be caused by lipid peroxidation, as lipophilic antioxidants, such as Ferrostatin-1 (Fer-1), can also prevent cell death.[64] Despite the growing recognition of the importance of ferroptosis as a cell death process, precise mechanisms linking labile iron pools and ferroptotic pathways remain insufficiently understood, in part due to a relative lack of tools for directly assaying labile Fe(II) in living specimens.[65]

Building on the demonstrated ability of FIP-1 to detect endogenous changes in labile Fe(II) in MDA-MB-231 cells (Figure 3), we turned our attention to linking labile iron fluxes to this model for ferroptosis. We observed that MDA-MB-231 cells begin to undergo exponential cell death when treated with 1.25 μM 35MEW28 (a recently reported inducer of ferroptosis)[66] after 10−12 h. For labile iron detection, we imaged cells using FIP-1 at various time points after treatment with 35MEW28 (Figure 4). Interestingly, we observed that the Green/FRET ratio increased 2 h after treatment as compared to the vehicle control and the signal further increased over time (Figure 4a, b). To validate that the ratiometric fluorescence response was derived from changes in the labile iron pool, we coincubated cells with 35MEW28 and 100 μM DFO. Confocal microscopy measurements at the 8 h time point no longer revealed an increased Green/FRET ratio (Figure 4c) compared to control (Figure 4a). However, when the cells are cotreated with 35MEW28 and the lipophilic antioxidant Fer-1, which blocks ferroptosis downstream of where we hypothesize a ferrous iron elevation to occur, we observe a Green/FRET ratio that is equivalent to cells treated with 35MEW28 alone (Figure 4d). As such, the data are consistent with the model that Fer-1 does not alter the mobilization of Fe(II) and indicates that the observed change in Green/FRET ratio is not simply an artifact of the process of ferroptosis. Taken together, these imaging results suggest that treatment with 35MEW28 may alter iron homeostasis to increase labile Fe(II) levels, serving as direct evidence that ferroptosis may be altering labile Fe(II) levels.

CONCLUDING REMARKS

To summarize, we have presented the design, synthesis, characterization, and biological applications of FIP-1, a unique first-generation chemical probe for ratiometric detection of Fe(II). FIP-1 operates by a reactivity mechanism in which Fe(II)-dependent cleavage of a bioinspired endoperoxide linker between donor and acceptor fluorophores modulates FRET. FIP-1 is responsive to Fe(II) in aqueous buffer with good metal- and oxidation state-selectivity and can report on changes in levels of labile Fe(II) pools in HEK 293T cells in a dose-dependent manner. Moreover, aided by its ratiometric response, this synthetic probe can be used to assay relative levels of labile iron across multiple cell types, as demonstrated by comparisons between normal and cancer cell lines under basal and chelator-treated conditions. Finally, FIP-1 provides direct evidence for changes in labile iron status during ferroptosis, opening the door to studies of dynamic iron signaling during this newly recognized form of cell death and other biological processes.

Even as a first-generation probe, FIP-1 offers some potential advantages when compared to recently described reaction-based probes for Fe(II), including IP1[23] and RhoNox-1[24] along with puromycin probe Trx-puro.[47] In contrast to IP1 and RhoNox-1, which are both turn-on probes, FIP-1 exhibits a ratiometric response to Fe(II), enabling internal correction for potential variations in dye concentrations and light input/output. In addition, compared to IP1, which requires an oxygen-dependent reaction in a three-component system (Fe/dye/O_2) to release a fluorescent product, the fluorescence readout of FIP-1 directly reports on Fe(II)-mediated cleavage. Finally, Trx-puro boasts excellent sensitivity based on its related trioxolane trigger, but this immunostaining readout is not amenable to real-time imaging in living cells like FIP-1. The synergistic development and application of FIP-1 and new chemical tools in this direction to study transition metal signaling are the focus of current efforts.

EXPERIMENTAL METHODS

General Methods. Reactions using moisture- or air-sensitive reagents were carried out in flame-dried glassware under an inert atmosphere of N_2. Solvent was passed over activated alumina and stored over activated 3 Å molecular sieves before use when dry solvent was required. All other commercially purchased chemicals were used as received (without further purification). 2-Adamantanone-5-carboxylic acid was purchased from Oakwood Products, Inc. (Estill, SC); hydroxylamine methyl ester hydrochloride and 1,4-cyclohexanedione were purchased from AK Scientific (Union City, CA); all other reagents were purchased from Sigma-Aldrich (St. Louis, MO). 5-Aminomethyl fluorescein (5-AMF) was prepared according to published procedures.[50] Cy3 was prepared according to published procedures.[51] SiliCycle 60 F254 silica gel (precoated sheets, 0.25 mm thick) were used for analytical thin layer chromatography and visualized by fluorescence quenching under UV light. Silica gel P60

DOI: 10.1021/jacs.6b08016
J. Am. Chem. Soc. 2016, 138, 14338−14346

(SiliCycle) was used for column chromatography. ^{1}H and ^{13}C NMR NMR spectra were collected at 298 K in $CDCl_3$ or CD_3OD (Cambridge Isotope Laboratories, Cambridge, MA) on Bruker AVQ-400, AVB-400, AV-500, or AV-600 at the College of Chemistry NMR Facility at the University of California, Berkeley or on Bruker 900 at the QB3 Central California 900 MHz NMR Facility. All chemical shifts are reported in the standard notation of δ parts per million relative to residual solvent peak at 7.26 ($CDCl_3$) or 3.31 (CD_3OD) for ^{1}H and 77.16 ($CDCl_3$) or 49.00 (CD_3OD) for ^{13}C as an internal reference. Splitting patterns are indicated as follows: br, broad; s, singlet; d, doublet; t, triplet; m, multiplet; dd, doublet of doublets. Low-resolution electrospray mass spectral analyses were carried out using a LC−MS (Agilent Technology 6130, Quadrupole LC−MS or Advion expression-L Compact Mass Spectrometer). High-resolution mass spectral analyses (ESI-MS) were carried out at the College of Chemistry Mass Spectrometry Facility at the University of California, Berkeley.

5-(Methoxycarbonyl)-2-adamantanone, 2. Thionyl chloride (0.450 mL, 6.17 mmol, 2.4 equiv) was added slowly to dry MeOH (26 mL) at 0 °C, and this was stirred for 15 min at this temperature. 2-adamantanone-5-carboxylic acid (0.5 g, 2.57 mmol, 1 equiv) was then added portion-wise over 5 min, also at 0 °C. The reaction mixture was allowed to warm to room temperature and was further stirred overnight. The reaction was then concentrated and loaded directly on silica gel for purification by flash column chromatography (0 → 35% EtOAc/Hex) to yield **2** (0.415 g, 78% yield) as a white solid. ^{1}H NMR (400 MHz, $CDCl_3$) δ (ppm): 3.48 (s, 3 H), 2.38 (s, 2 H), 2.00−1.77 (m, 11 H). ^{13}C NMR (101 MHz, $CDCl_3$) δ (ppm): 215.88, 175.71, 51.63, 45.47, 39.82, 37.98, 37.51, 26.98. LRMS calcd. for $C_{12}H_{16}O_3$ $[M + H]^+$ 209.11, found 209.2.

Oxime Ether 3. 5-(Methoxycarbonyl)-2-adamantanone (0.114 g, 0.55 mmol, 1 equiv) and hydroxylamine methyl ester hydrochloride (0.050 g, 0.6 mmol, 1.1 equiv) were added to a round-bottom flask in pyridine (2 mL), and the reaction mixture was stirred at room temperature for 3 h. After 3 h, the reaction was acidified to pH 7 by addition of 1 M HCl, then EtOAc was added. The organic layer was washed with 1 M aq HCl (2 × 15 mL) and the combined aq layer was then extracted with EtOAc (3 × 15 mL), washed with brine, dried over Na_2SO_4 filtered, and concentrated in vacuo to yield **3** (0.130 g, 100%). ^{1}H NMR (400 MHz, $CDCl_3$) δ (ppm): 3.76 (s, 3 H), 3.60 (s, 3 H), 3.49 (s, 1 H), 2.57 (s, 1 H), 2.05−1.78 (m, 12 H). ^{13}C NMR (101 MHz, $CDCl_3$) δ (ppm): 176.75, 165.48, 61.07, 51.85, 40.73, 40.00, 38.66, 38.00, 36.57, 35.57, 28.76, 27.65. LRMS calcd. for $C_{13}H_{19}NO_3$ $[M + H]^+$ 238.14, found 238.2.

Endoperoxide 4. Oxime ether **3** (1.462 g, 6.16 mmol, 1 equiv) and 1,4-cyclohexanedione (1.384 g, 12.32 mmol, 2 equiv) were dried in vacuo, then were added to a flame-dried 100 mL Schlenk flask. Dry CCl_4 (50 mL) and dry CH_2Cl_2 (25 mL) were added and the reaction mixture was stirred at 0 °C for 5 min before bubbling ozone through solution for 2.5 h at this temperature. At this point, the reaction was purged of ozone, warmed to room temperature, and concentrated. The concentrate was loaded directly on silica gel for purification by silica chromatography (0 → 25% EtOAc/Hex) to yield **4** (0.680 g, 33%) as a pale-yellow solid. **4** was isolated as a mixture of diastereomers. ^{1}H NMR (400 MHz, $CDCl_3$) δ (ppm): 3.67−3.64 (m, 3 H), 2.51 (t, 3 H), 2.22−2.10 (m, 8 H), 2.03−1.83 (m, 7 H), 1.75−1.65 (m, 2 H). ^{13}C NMR (101 MHz, $CDCl_3$) δ (ppm): 209.25, 209.20, 177.18, 177.10, 111.46, 111.42, 107.44, 107.41, 51.92, 45.91, 40.27, 39.95, 39.55, 38.46, 38.23, 38.16, 37.89, 36.44, 36.26, 36.03, 35.88, 33.85, 33.75, 33.14, 33.12, 27.41, 26.62, 26.22. LRMS calcd. for $C_{18}H_{24}O_6$ $[M + H]^+$ 337.16, found 337.2.

Endoperoxide Amine 5. Endoperoxide **4** (0.1485 g, 0.4415 mmol, 1 equiv) and NH_4OAc (0.340 g, 4.415 mmol, 10 equiv) were added to a round-bottom flask in dry MeOH (8 mL), and this was stirred for 5 min at room temperature before adding $NaBH_3CN$ (0.0194 g, 0.31 mmol, 0.7 equiv). The reaction mixture was stirred at room temperature overnight. The reaction was quenched by addition of 150 mL water and the MeOH was removed by concentrating in vacuo. At this point, the reaction mixture was basified (brought to pH 8) by addition of 5 M NaOH then was extracted three times with $CHCl_3$, washed with aq sat NaCl, dried over Na_2SO_4, filtered and the solvent was removed by rotary evaporation, at which point the concentrate was loaded directly on silica gel for purification by silica chromatography (50 → 100% EtOAc/Hex) → 0 → 10% MeOH in CH_2Cl_2) to yield 5 (0.085 g, 56%). ^{1}H NMR (600 MHz, $CDCl_3$) δ (ppm): 3.643 (t, 3 H), 2.524 (m, 1 H), 2.232−1.493 (m, 23 H). LRMS calcd. for $C_{18}H_{27}NO_5$ $[M + H]^+$ 338.19, found 338.2.

Endoperoxide Carboxylic Acid 6. Endoperoxide-free amine **5** (0.1377 g, 0.41 mmol, 1 equiv) was dissolved in 2 mL THF, then lithium hydroxide (0.015 g, 0.612 mmol, 1.5 equiv) was added in 2 mL water. This was stirred overnight, then was concentrated to yield **6** (0.140 g, 100%) which was carried on to the next step without without further purification. ^{1}H NMR (600 MHz, CD_3OD) δ (ppm): 2.708 (m, 1 H), 2.205−1.369 (m, 27 H) ^{13}C NMR (101 MHz, $CDCl_3$) 185.88, 109.46, 58.29, 42.36, 40.47, 38.49, 38.02, 37.92, 35.13, 18.42. LRMS calcd. for $C_{12}H_{16}O_3$ $[M + H]^+$ 324.17, found 324.2.

Cy3 NHS Ester 8. Cy3 (0.520 g, 0.91 mmol, 1.0 equiv) was dried under high vacuum for 30 min and dissolved in 10 mL dry DMF. Disuccinimidyl carbonate (DSC) (0.350 g, 1.37 mmol, 1.5 equiv), DMAP (0.0021 mg, 0.02 mmol, 0.02 equiv) and NEt_3 (254 μL, 0.184 g, 1.82 mmol, 2.0 equiv) were added and the dark red solution was stirred at room temperature overnight. An amount of 20 mL CH_2Cl_2 were added and the organic phase was washed with slightly acidic water (3 × 10 mL). The aqueous phases were re-extracted with CH_2Cl_2 (15 mL). Combined organic phases were dried over $MgSO_4$, filtered and the solvent was removed by rotary evaporation. Purification by flash column chromatography (5% ^{i}PrOH in CH_2Cl_2) yielded Cy3-NHS ester as a dark purple solid. ^{1}H NMR (600 MHz, $CDCl_3$) δ (ppm): 8.35 (t, 1H), 7.33 (t, 4H), 7.15 (m, 6H), 4.22 (t, 2H), 3.72 (s, 3H), 2.77 (s, 4 H), 1.92 (d, 4H), 1.65 (s, 12H). ^{13}C NMR (101 MHz, $CDCl_3$) 174.15, 173.62, 169.11, 168.33, 150.77, 142.56, 141.78, 140.39, 140.34, 128.85, 128.74, 125.26, 125.21, 122.03, 121.96, 110.93, 110.77, 104.87, 104.59, 53.43, 48.85, 48.81, 44.14, 32.06, 30.46, 28.07, 27.97, 26.25, 25.57,21.86. LRMS calcd. for $C_{33}H_{38}O_4N_3$ $[M + H]^+$ 540.3 found 540.5.

Cy3 Linker 7. Endoperoxide-carboxylic acid **6** (0.048 g, 0.15 mmol, 1.0 equiv) and Cy3-NHS ester **8** (0.100 mg, 0.15 mmol, 1.0 equiv) were dried under high vacuum for 10 min and dissolved in 1 mL dry DMF. Dry NEt_3 (42 μL, 0.030 g, 0.30 mmol, 2.0 equiv) was added and the dark red solution was warmed to 30 °C and stirred overnight. The solvent was removed by vacuum distillation and the crude concentrate was purified by flash column chromatography (gradient of 0 → 20% MeOH in CH_2Cl_2) to yield Cy3-linker **7** (0.038 g, 0.04 mmol, 29%) as a dark red solid and as a mixture of diastereomers. ^{1}H NMR (500 MHz, CD_3OD) δ (ppm): 8.56 (t, 1H), 7.57 (d, 2H), 7.46 (m, 2H), 7.42−7.28 (m, 4H), 6.50 (m, 2H), 4.19 (bt, 2H), 3.73 (m, 3 H), 2.29 (bt, 2 H), 2.21 (m, 2 H), 2.11−1.42 (m, 46) ^{13}C NMR (226 MHz, CD_3OD) 176.97, 176.21, 175.98, 175.04, 152.34, 152.20, 144.26, 143.71, 142.39, 142.34, 130.19, 127.02, 126.90, 123.76, 123.60, 112.62, 112.52, 111.95, 109.44, 104.24, 104.0, 103.94, 103.82, 45.08, 44.81, 41.18, 39.70, 38.06, 37.78, 37.70, 37.57, 36.73, 36.38, 34.93, 34.76, 33.89, 33.66, 33.27, 32.05, 30.98, 30.63, 30.54, 30.37, 28.54, 28.37, 28.05, 27.91, 27.62, 27.12,24.33, 23.94. LRMS calcd. for $C_{46}H_{58}O_6N_3$ $[M + H]^+$ 748.43, found 749.

FRET Iron Probe 1 (FIP-1). Cy3-linker **7** (0.035 g, 0.040 mmol, 1.0 equiv) and HBTU (0.017 g, 0.044 mmol, 1.1 equiv) were dried under high vacuum for 1 h and dissolved in 1 mL dry DMF. After addition of dry DIPEA (10 μL, 0.0072 g, 0.56 mmol, 1.4 equiv), the solution was stirred for 1 h. 5-aminomethyl fluorescein (0.022 g, 0.06 mmol, 1.5 equiv) was dried under high vacuum for 90 min, dissolved in 1 mL dry DMF and dry DIPEA (20 μL, 0.0145 g, 1.1 mmol, 2.8 equiv) then transferred to the solution containing the activated ester. The resulting solution was stirred overnight. An amount of 10 mL of saturated, aqueous NH_4Cl and 10 mL water were added and the aqueous phase was extracted with EtOAc (4 × 10 mL). The combined organic phases were washed with water (2 × 10 mL) and brine. The solvent was removed by rotary evaporation and purified by flash column chromatography (gradient of 0 → 15% MeOH in CH_2Cl_2). Final purification was achieved by UHPLC (gradient of 53% H_2O supplemented with 0.05% formic acid (FA) in MeCN supplemented

DOI: 10.1021/jacs.6b08016
J. Am. Chem. Soc. 2016, 138, 14338−14346

with FA → 47% H_2O supplemented with 0.05% formic acid (FA) in MeCN supplemented with FA over 13 min → 100% MeCN supplemented with FA over 2 min, from 13 to 15 min). FRET Iron Probe 1 (FIP-1) (0.00341 g, 0.0028 mmol, 7%) was obtained as a red film. ^{1}H NMR (500 MHz, CD_3OD) δ (ppm): 7.87 (s, 1 H), 7.55 (d, 2 H), 7.49 (d, 1 H), 7.44 (t, 2H), 7.37 (t, 2 H), 7.31 (t, 2H), 7.16 (d, 1 H), 7.00 (s, 2 H), 6.65 (s, 2 H), 6.59 (dd, 2 H), 6.39 (m, 2 H), 4.62 (s, 1 H), 4.50 (s, 2 H), 4.15 (t, 2 H), 3.70 (s, 3 H), 2.24 (t, 2 H), 2.10 (d, 2 H), 1.87−1.73 (m, 29 H), 1.62 (d, 2 H), 1.54 (d, 2 H), 1.44 (m, 2 H). ^{13}C NMR (226 MHz, CD_3OD) 179.77, 176.75, 176.04, 175.83, 174.82, 170.19, 169.38, 163.24, 163.09, 162.93, 152.00, 144.12, 144.02, 143.51, 143.35, 142.15, 132.42, 131.37, 130.00, 129.83, 126.91, 126.74, 112.44, 112.26, 111.56, 111.82, 103.78, 103.91, 103.73, 103.6, 69.95, 60.95, 50.67, 50.63, 50.44, 48.15, 44.88, 44.62, 43.48, 39.26, 37.57, 37.52, 37.50, 36.21, 34.84, 34.48, 33.69, 33.40, 33.09, 30.79, 30.36, 30.48, 3040, 30.15, 28.33, 28.17, 27.80, 27.47, 24.96, 24.19, 24.15, 23.75, 14.44, 11.40. HRMS calcd. for $C_{67}H_{71}O_{10}N_4$ $[M + H]^+$ 1091.517, found 1091.518.

Spectroscopic Materials and Methods. All aqueous solutions were prepared using Milli-Q water, and all spectroscopic experiments were carried out in 50 mM HEPES, pH 7.4, unless otherwise noted. All spectroscopic experiments were carried out using freshly prepared aliquots, and solutions were prepared in an anaerobic chamber (MBraun), unless otherwise noted. Water and buffer used for spectroscopic measurements were deoxygenated in three freeze−pump−thaw cycles on a Schlenk line. Absorption spectra were acquired on a Varian Cary 50 spectrophotometer, and fluorescence spectra were acquired using a Photon Technology International Quanta Master 4 L-format scan spectro-fluorometer equipped with an LPS-220B 75-W xenon lamp and power supply, A-1010B lamp housing with integrated igniter, switchable 814 photocounting/analog photomultiplier detection unit, and MD5020 motor driver. 1 cm × 1 cm quartz cuvettes (1.4 mL volume, Starna, capped) were used for obtaining absorption and fluorescence spectra. For all fluorescence response to iron(II) studies, aqueous solutions of $Fe(NH_4)_2(SO_4)_2(H_2O)_6$ (FAS) (Sigma) were used. For metal selectivity studies, aqueous metal solutions of $MgCl_2{\cdot}4H_2O$ (EMD Millipore), $CaCl_2{\cdot}2H_2O$ (EMD Millipore), $NiCl_2{\cdot}6H_2O$ (Sigma), $ZnCl_2$ (Sigma), $CuCl_2{\cdot}2H_2O$ (Baker and Adamson), $CoCl_2{\cdot}6H_2O$ (Sigma), $MgCl_2{\cdot}6H_2O$ (Sigma), NaCl (Sigma), $[Cu(CH_3CN)_4]PF_6$ (Sigma), KCl (Sigma), and $FeCl_3$ (Sigma) were used. GSH (Sigma) and myoglobin (Sigma) were used for selectivity studies.

Fluorescence Responses to Iron. 999 μL of a 1 μM solution of FIP-1 was prepared by diluting a 1 mM DMSO stock solution of FIP-1 into 50 mM HEPES (pH 7.4) in a 1 cm × 1 cm capped quartz cuvette. The probe solution was incubated at 37 °C for 5 min, then 1 μL of 10 mM stock solution of ferrous ammonium sulfate (FAS) (freshly prepared by diluting FAS into deoxygenated Milli-Q water) was added to yield a final concentration of 10 μM. The mixture was then vortexed in the capped cuvette, then the t = 0 spectrum was acquired. Emission spectra (λ_{ex} = 488 nm, λ_{em} = 500−620 nm) were collected at t = 0, 5, 10, 15, 20, 30, 45, 60, and 90 min. Temperature was maintained at 37 °C throughout the experiment by incubating cuvettes in a heated water bath.

Dose Dependence *In Vitro*. 999 μL of a 1 μM solution of FIP-1 was prepared by diluting a 1 mM DMSO stock solution of FIP-1 into 50 mM HEPES (pH 7.4) in a 1 cm × 1 cm capped quartz cuvette. The probe solution was incubated at 37 °C for 5 min. Then 1 or 5 μL of a 1 mM stock solution of FAS (freshly prepared by diluting FAS into deoxygenated Milli-Q water) was added to yield a final concentration of 1 or 5 μM, or 1 or 2 μL of a 10 mM stock solution of FAS (freshly prepared by diluting FAS into deoxygenated Milli-Q water) was added to yield a final concentration of 10 or 20 μM. The mixture was then vortexed in the capped cuvette, then the t = 0 spectrum was acquired. Emission spectra (λ_{ex} = 488 nm, λ_{em} = 500−620 nm) were collected at t = 0, 5, 10, 15, 20, 30, 45, 60, and 90 min. Temperature was maintained at 37 °C throughout the experiment by incubating cuvettes in a heated water bath.

Metal, GSH, and Myoglobin Selectivity Experiments. A 2 μM solution of FIP-1 was prepared by diluting a 1 mM DMSO stock solution of probe into 4.990 mL HEPES. 500 μL of this solution were added to ten 1 cm × 1 cm capped quartz cuvettes, then the cuvettes were placed in a 37 °C water bath for 5 min. After 5 min, 500 μL of a solution of the metal of interest was added to the cuvette to bring the concentration of transition metals to 10 μM and the concentration of alkaline earth/alkali metals to 1 mM. For GSH experiments, a 10 mM solution of GSH was prepared in HEPES buffer and this was brought to neutral pH by adding 1 M NaOH. 500 μL of this solution was added to 500 μL FIP-1 in HEPES solution for a final GSH concentration of 5 mM. 500 μL of buffer was added to one cuvette, and this sample served as the blank throughout the experiment. The mixture was then vortexed in the capped cuvette, then the t = 0 spectrum was acquired for the blank sample. Spectra were taken at t = 60 min. For myoglobin experiments, a 1 mM solution of myoglobin was prepared in HEPES buffer. An amount of 10 μL of this solution was added to 1 mL FIP-1 in HEPES solution for a final myoglobin concentration of 10 μM. The mixture was then vortexed in the capped cuvette, then the t = 0 spectrum was acquired for the blank sample. Spectra were taken at t = 60 min.

Cell Culture Procedures. Cells were maintained by the UC Berkeley Tissue Culture Facility. HEK 293T, MDA-MB-231, and U-2OS cells were maintained as a monolayer in exponential growth at 37 °C in a 5% CO_2 atmosphere in Dulbecco's Modified Eagle Medium (DMEM, Gibco) supplemented with 10% fetal bovine serum (FBS, Hyclone), and glutamax (Gibco). One day before imaging, HEK 293T cells were passaged and plated in phenol red-free medium on poly D-lysine-coated 4-well Lab Tek borosilicate chambered coverglass slides (Nunc) at 1.8 × 10^5 per well. HEK 293T cells were allowed to grow to between 60 and 70% confluence before imaging. MCF-10A cells were maintained in DMEM/F12 (500 mL, Invitrogen) with 5% horse serum (25 mL, Invitrogen), insulin (500 μL from 10 mg/mL stock), cholera toxin (50 μL, from 1 mg/mL stock), hydrocortisone (250 μL, from 1 mg/mL stock), EGF (100 μL, from 100 μg/mL stock) and HEPES. One day before imaging, MCF10A, MDA-MB-231, and U-2OS cells cells were passaged and plated on 4-well Lab Tek borosilicate chambered coverglass slides (Nunc) and allowed to grow to between 60 and 80% confluence before imaging.

Confocal Fluorescence Imaging Experiments. A Zeiss laser scanning microscope 710 with a 20x objective lens and Zen 2009 software (Carl Zeiss) was used for all confocal fluorescence imaging experiments. FIP-1 was excited using a 488 nm Ar laser ("Green" channel and "FRET" channel) and 543 nm HeNe laser (red channel). "Green" emission was collected using a META detector between 500 and 535 nm, "FRET" emission was collected using a META detector between 555 and 611 nm, and "red" emission was collected using a META detector between 555 and 611 nm. Hoechst 33342 was excited with a 405 nm diode laser, and emission was collected using a META detector between 410 and 590 nm. Cells were kept at 37 °C throughout imaging experiments, and HBSS (containing calcium and magnesium) was used as the imaging buffer in all experiments. Image analysis and quantification was performed using ImageJ (National Institutes of Health). Quantification of fluorescence intensities were conducted as described previously.[66] Statistical analyses for multiple comparisons were carried out through one-way ANOVA with the Bonferroni correction using the software R.

Fe(II) Supplementation and Chelation Experiments. 250 μM DFO or 1 mM BPS was added to DMEM media containing 10% FBS and glutamax in chambers containing cells and incubated at 37 °C for 8 h. At this point, media in these wells was replaced with 250 μM DFO or 1 mM BPS containing DMEM media (without FBS and glutamax) and incubated for 90 min at 37 °C. DMEM media in nontreated wells was aspirated from chambers containing cells and this was replaced with DMEM media containing 100 μM FAS (prepared from a 20 mM FAS solution in water) or DMEM media alone and this was incubated for 90 min at 37 °C. After 90 min, DMEM media was aspirated and cells were washed one time with 500 μL HBSS. Then 500 μL HBSS containing 10 μM FIP-1 (diluted from 5 mM stock) was added to each well and this was incubated at 37 °C for 90 min. At this point, buffer was removed and each well was washed 2× with 500 μL HBSS. Then 500 μL of HBSS were added and snapshot images were taken. Cells

DOI: 10.1021/jacs.6b08016
J. Am. Chem. Soc. 2016, 138, 14338−14346

were then incubated with 1 μM Hoechst 33342 at 37 °C for 10 min prior to imaging nuclear staining.

Ferroptosis Experiments. MDA-MB-231 cells were cultured in DMEM supplemented with 10% fetal bovine serum (FBS, Hyclone), glutamax (Gibco), and 1% nonessential amino acids (NEAA, Gibco). One day before the experiment, cells were passaged and plated in phenol-red free medium in 4-well Lab Tek borosilicate chambered coverglass slides (Nunc). Media was aspirated and was replaced with 100 μL DMEM media containing 10% FBS and glutamax and either DMSO vehicle, 1.25 μM 35MEW28,[66] 1.25 μM 35MEW28 + 1 μM ferrostatin-1 (Fer-1), or 1.25 μM 35MEW28 + 100 μM DFO for 8 h, at which point media was removed and was washed one time with 500 μL HBSS. Then 500 μL HBSS containing 10 μM FIP-1 (diluted from a 5 mM stock in DMSO) was added to each well and this was incubated at 37 °C for 90 min. At this point, buffer was removed and each well was washed 2× with 500 μL HBSS, then 500 μL of HBSS were added and snapshot images were taken.

■ ASSOCIATED CONTENT

Supporting Information

The Supporting Information is available free of charge on the ACS Publications website at DOI: 10.1021/jacs.6b08016.

Additional experimental details, including Fe(II) dose dependence, Inductively Coupled Plasma Mass Spectometry (ICP-MS), and Cell Viability procedures, supplemental figures, and NMR spectra (PDF)

■ AUTHOR INFORMATION

Corresponding Author

*chrischang@berkeley.edu

Notes

The authors declare no competing financial interest.

■ ACKNOWLEDGMENTS

We thank the NIH (GM79465) for supporting this work. A.T.A was partially supported by an NSF Graduate Fellowship and a Chemical Biology Training Grant from the NIH (T32 GM066698). C.J.C. is an Investigator of the Howard Hughes Medical Institute. We thank Alison Killilea and Carissa Tasto (UC Berkeley Tissue Culture Facility) for expert technical assistance. We thank Thomas Brewer, Cheri Ackerman, Marie Heffern, and Lakshmi Krishnamoorthy, as well as Ben Spangler and Adam Renslo, for helpful discussions. We thank Megan Conlon and Scott Dixon for providing 35MEW28.

■ REFERENCES

(1) Lippard, S. J.; Berg, J. M. *Principles of Bioinorganic Chemistry*; University Science Book: Mill Valley, CA, 1994.

(2) Hentze, M. W.; Muckenthaler, M. U.; Andrews, N. C. *Cell* **2004**, *117*, 285.

(3) Theil, E. C.; Goss, D. J. *Chem. Rev.* **2009**, *109*, 4568.

(4) Aisen, R.; Enns, C.; Wessling-Resnick, M. *Int. J. Biochem. Cell Biol.* **2001**, *33*, 940.

(5) Cammack, R.; Wrigglesworth, J. M.; Baum, H. In *Transport and Storage*; Ponka, P., Schulman, H. M., Woodworth, R. C., Richter, G. W., Eds.; CRC Press: 1989; p 17.

(6) Johnson, D. C.; Dean, D. R.; Smith, A. D.; Johnson, M. K. *Annu. Rev. Biochem.* **2005**, *74*, 248.

(7) Winterbourn, C. C. *Toxicol. Lett.* **1995**, *82/83*, 969.

(8) James, S. A.; Robert, B. R.; Hare, D. J.; de Jonge, M. D.; Birchall, I. E.; Jenkin, N. L.; Cherny, R. A.; Bush, A. I.; McColl, G. *Chem. Sci.* **2015**, *6*, 2952.

(9) von Haehling, S.; Jankowska, E. A.; van Veldhuisen, D. J.; Ponikowski, P.; Anker, S. D. *Nat. Rev. Cardiol.* **2015**, *12*, 659.

(10) Hare, D.; Ayton, S.; Bush, A.; Lei, P. *Front. Aging Neurosci.* **2013**, *5*, 34.

(11) Gerlach, M.; Ben-Shachar, D. B.; Riedere, P.; Youdim, M. B. H. *J. Neurochem.* **1994**, *63*, 793.

(12) Torti, S. V.; Torti, F. M. *Nat. Rev. Cancer* **2013**, *13*, 342.

(13) Wu, K. J.; Polack, A.; Dala-Favera, R. *Science* **1999**, *283*, 676.

(14) Pinnix, Z. K.; Miller, L. D.; Wang, W.; D'Agostino, R. J.; Kute, T.; Willingham, M. C.; Hatcher, H.; Tesfay, L.; Sui, G.; Di, X.; Torti, S. V.; Torti, F. M. *Sci. Transl. Med.* **2010**, *2*, 43ra56.

(15) Toyokuni, S. *Cancer Sci.* **2009**, *100*, 9.

(16) Carter, K. P.; Young, A. M.; Palmer, A. E. *Chem. Rev.* **2014**, *114*, 4564.

(17) Domaille, D. W.; Que, E. L.; Chang, C. J. *Nat. Chem. Biol.* **2008**, *4*, 168.

(18) Irving, H.; Williams, R. J. P. *J. Chem. Soc.* **1953**, 3192.

(19) Kemlo, J. A.; Shepherd, T. M. *Chem. Phys. Lett.* **1977**, *47*, 158.

(20) Varnes, A. W.; Dodson, R. B.; Wehry, E. L. *J. Am. Chem. Soc.* **1972**, *94*, 946.

(21) Breuer, W.; Epsztejn, S.; Millgram, P.; Cabnatchik, I. Z. *Am. J. Physiol.* **1995**, *268*, C1354.

(22) Kakhlon, O.; Cabantchik, Z. I. *Free Radical Biol. Med.* **2002**, *33*, 1037.

(23) Au-Yeung, H. Y.; Chan, J.; Chantarojsiri, T.; Chang, C. J. *J. Am. Chem. Soc.* **2013**, *135*, 15165.

(24) Hirayama, T.; Okuda, K.; Nagasawa, H. *Chem. Sci.* **2013**, *4*, 1250.

(25) Niwa, M.; Hirayama, T.; Okuda, K.; Nagasawa, H. *Org. Biomol. Chem.* **2014**, *12*, 6590.

(26) Chan, J.; Dodani, S. C.; Chang, C. J. *Nat. Chem.* **2012**, *4*, 973.

(27) Aron, A. T.; Ramos-Torres, K. M.; Cotruvo, J. J. A.; Chang, C. J. *Acc. Chem. Res.* **2015**, *48*, 2434.

(28) Chen, X.; Tian, X.; Shin, I.; Yoon, J. *Chem. Soc. Rev.* **2011**, *40*, 4783.

(29) Yang, Y.; Zhao, Q.; Feng, W.; Li, F. *Chem. Rev.* **2013**, *113*, 192.

(30) Cho, D. G.; Sessler, J. L. *Chem. Soc. Rev.* **2009**, *38*, 1647.

(31) Zlokarnik, G.; Negulescu, P. A.; Knapp, T. E.; Mere, L.; Burres, N.; Feng, L.; Whitney, M.; Roemer, K.; Tsein, R. Y. *Science* **1998**, *279*, 84.

(32) Lee, M. H.; Kim, J. S.; Sessler, J. L. *Chem. Soc. Rev.* **2015**, *44*, 4185.

(33) Grynkiewicz, G.; Poenie, M.; Tsien, R. Y. *J. Biol. Chem.* **1985**, *260*, 3440.

(34) Harootunian, A. T.; Kao, J. P. Y.; Ecker, B. K.; Tsien, R. Y. *J. Biol. Chem.* **1989**, *264*, 19458.

(35) Borstnik, K.; Paik, I.; Shapiro, T.; Posner, G. H. *Int. J. Parasitol.* **2002**, *32*, 1661.

(36) Wang, X. *Bioorg. Med. Chem. Lett.* **2009**, *19*, 4542.

(37) Deu, E.; Chen, I. T.; Lauterwasser, E. M.; Valderramos, J.; Li, H.; Edgington, L. E.; Renslo, A. R.; Bogyo, M. *Proc. Natl. Acad. Sci. U. S. A.* **2013**, *110*, 18244.

(38) Fontaine, S. D.; Spangler, B.; Gut, J.; Lauterwasser, E. M.; Rosenthal, P. J.; Renslo, A. R. *ChemMedChem* **2015**, *10*, 47.

(39) Fontaine, S. D.; DiPasquale, A. G.; Renslo, A. R. *Org. Lett.* **2014**, *16*, 5776.

(40) Abrams, R. P.; Carroll, W. L.; Woerpel, K. A. *ACS Chem. Biol.* **2016**, *11*, 1305.

(41) Creek, D. J.; Charman, W. N.; Chiu, F. C.; Prankerd, R. J.; Dong, Y.; Vennerstrom, J. L.; Charman, S. A. *Antimicrob. Agents Chemother.* **2008**, *52*, 1291.

(42) Creek, D. J.; Charman, W. N.; Chiu, F. C. K.; Orankerd, R. J.; McCullough, K. J.; Dong, Y.; Vennerstrom, J. L.; Charman, S. A. *J. Pharm. Sci.* **2007**, *96*, 2945.

(43) Tang, Y.; Dong, Y.; Wang, X.; Sriraghavan, K.; Wood, J. K.; Vennerstrom, J. L. *J. Org. Chem.* **2005**, *70*, 5103.

(44) Chang, C. J. *Nat. Chem. Biol.* **2015**, *111*, 744.

(45) Tang, Y.; Dong, Y.; Wang, X.; Sriraghavan, K.; Wood, J. K.; Vennerstrom, J. L. *J. Org. Chem.* **2005**, *70*, 5103.

(46) Creek, D. *J. Pharm. Sci.* **2007**, *96*, 2945.

DOI: 10.1021/jacs.6b08016
J. Am. Chem. Soc. 2016, 138, 14338−14346

(47) Spangler, B.; Morgan, C. W.; Fontaine, S. D.; Vander Wal, M. N.; Chang, C. J.; Wells, J. A.; Renslo, A. R. *Nat. Chem. Biol.* **2016**, *12*, 680.
(48) Norman, D. G.; Grainger, R. J.; Uhrin, D.; Tilley, D. M. J. *Biochemistry* **2000**, *39*, 6317.
(49) Li, X.; Yu, J.; Zhu, Q.; Qian, L.; Li, L.; Zheng, Y.; Yao, S. Q. *Analyst* **2014**, *139*, 6092.
(50) Mattingly, P. G. 5(6)-methyl substituted fluorescein derivatives. U.S. Patent EP0635020 A1, Jan 25, 1995.
(51) Korbel, G. A.; Lalic, G.; Shair, M. D. *J. Am. Chem. Soc.* **2001**, *123*, 361.
(52) Cerchiaro, G.; Manieri, T. M.; Bertuchi, F. R. *Metallomics* **2013**, *5*, 1336.
(53) Epsztejn, S.; Kakhlon, O.; Glickstein, H.; Breuer, W.; Cabantchik, Z. I. *Anal. Biochem.* **1997**, *248*, 31.
(54) Ramos-Torres, K. M.; Kolemen, S.; Chang, C. J. *Isr. J. Chem.* **2016**, DOI: 10.1002/ijch.201600023.
(55) Cotruvo, J. J. A.; Aron, A. T.; Ramos-Torres, K. M.; Chang, C. J. *Chem. Soc. Rev.* **2015**, *44*, 4400.
(56) Rubino, J. T.; Franz, K. J. *J. Inorg. Biochem.* **2012**, *107*, 129.
(57) Davis, A. V.; O'Halloran, T. V. *Nat. Chem. Biol.* **2008**, *4*, 148.
(58) Kim, B. E.; Nevitt, T.; Thiele, D. *Nat. Chem. Biol.* **2008**, *4*, 176.
(59) Torti, S. V.; Torti, F. M. *Cancer Res.* **2011**, *71*, 1511.
(60) Zhang, C.; Zhang, F. *Protein Cell* **2015**, *6*, 88.
(61) Bogdan, A. R.; Miyazawa, M.; Hashimoto, K.; Tsuji, Y. *Trends Biochem. Sci.* **2016**, *41*, 274.
(62) Dixon, S. J.; Stockwell, B. R. *Nat. Chem. Biol.* **2014**, *10*, 9.
(63) Yang, W. S.; Stockwell, B. R. *Chem. Biol.* **2008**, *15*, 234.
(64) Dixon, S. J.; Lemberg, K. M.; Lamprecht, M. R.; Skouta, R.; Zaitsev, E. M.; Gleason, C. E.; Patel, D. N.; Bauer, A. J.; Cantley, A. M.; Yang, W. S.; Morrison, B. I.; Stockwell, B. R. *Cell* **2012**, *149*, 1060.
(65) Dixon, S. J.; Stockwell, B. R. *Nat. Chem. Biol.* **2013**, *10*, 9.
(66) Dixon, S. J.; Patel, D. N.; Welsch, M.; Skouta, R.; Lee, E. D.; Hayano, M.; Thomas, A. G.; Gleason, C. E.; Tatonetti, N. P.; Slusher, B. S.; Stockwell, B. R. *eLife* **2014**, *3*, e02523.

NOTE ADDED AFTER ASAP PUBLICATION

This paper was published on October 21, 2016. Scheme 2 has been corrected and the paper was re-posted on October 24, 2016.

DOI: 10.1021/jacs.6b08016
J. Am. Chem. Soc. 2016, 138, 14338−14346